International Journal of Engineering Science and Advanced Technology (IJESAT)
Vol 26 Issue 11, November 2026
Received: 09-10-2026 Accepted: 13-11-2026 Published: 19-11-2026

Tribology of Hydrogen Fuelled Engines and Hydrogen Compression Systems

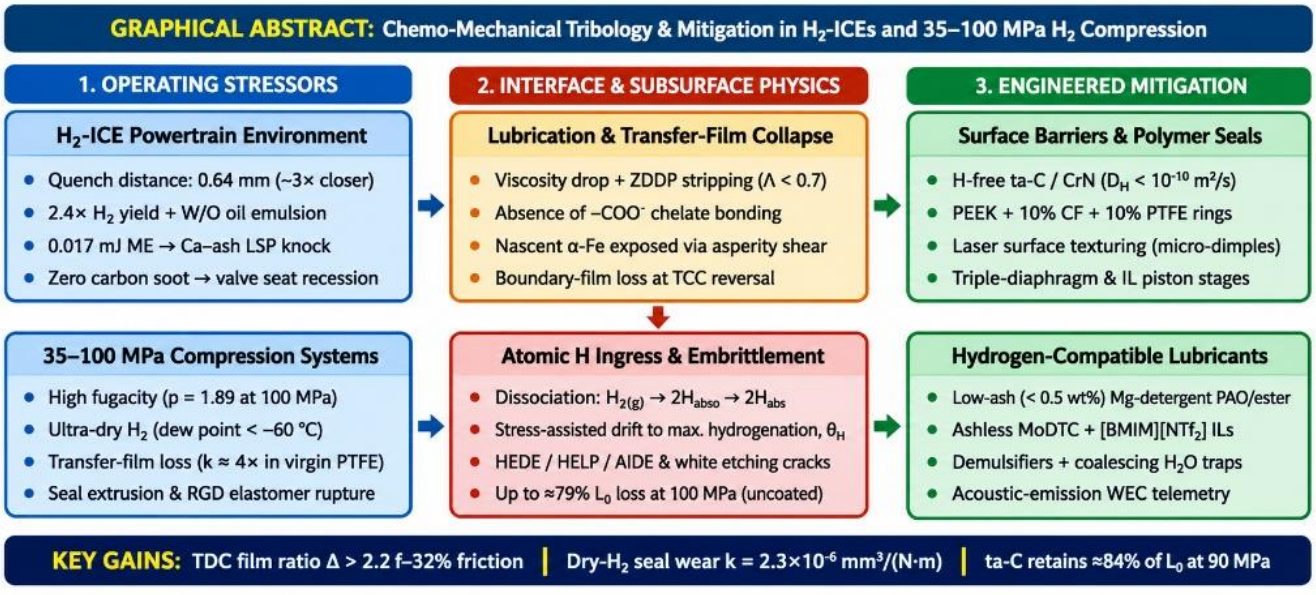
Gugulothu Shankar*

Assistant Professor, Department of Mechanical Engineering, Sri Chaitanya Institute of Technology and Research, Ponnekal, Khammam Rural, Khammam District, Telangana – 507170, India.

***Corresponding Email:** gugulothushankar1971@gmail.com

Abstract—The rapid decarbonization of heavy-duty transport, stationary power generation, and industrial energy storage relies heavily on hydrogen internal combustion engines (H_2-ICEs) and high-pressure hydrogen compression systems operating between 35 MPa and 100 MPa. Despite their zero-carbon tailpipe emissions and high thermodynamic efficiency, both technologies face severe tribological reliability bottlenecks arising from the unique physicochemical interactions of molecular and atomic hydrogen with metallic, polymeric, and lubricated interfaces. In H_2-ICEs, a 70% shorter flame quenching distance (0.64 mm versus 2.1 mm for gasoline) elevates top cylinder liner temperatures, accelerating lubricant evaporation and shifting the piston ring–cylinder liner (PRCL) contact into boundary lubrication (film parameter $\Lambda < 1$). Simultaneously, stoichiometric hydrogen combustion generates 2.4 times more water vapor per unit energy than hydrocarbon fuels, causing crankcase oil emulsification, additive hydrolysis, and zinc dialkyldithiophosphate (ZDDP) tribofilm stripping, while calcium-based detergents induce catastrophic low-speed pre-ignition (LSPI). Conversely, high-pressure reciprocating, diaphragm, and ionic-liquid hydrogen compressors operate under ultra-dry, oil-free gas environments (dew point < -60°C) where the absence of condensable moisture and oxygen inhibits the formation of stable polytetrafluoroethylene (PTFE) transfer films, increasing specific wear rates by up to an order of magnitude. Furthermore, nascent iron surfaces exposed by asperity shear catalyze dissociative H_2 chemisorption and stress-assisted lattice diffusion, triggering hydrogen-enhanced decohesion (HEDE), hydrogen-enhanced localized plasticity (HELP), and premature white etching crack (WEC) subsurface spalling. This paper synthesizes the multi-scale chemo-mechanical degradation mechanisms governing H_2-ICEs and hydrogen compressors, establishes coupled fugacity-modified Archard wear and elastohydrodynamic film formulations, benchmarks advanced self-lubricating polymer composites and hydrogen-barrier diamond-like carbon (ta-C/CrN) coatings, and presents an integrated system-level tribological mitigation roadmap.

Index Terms—*Hydrogen internal combustion engine (H_2-ICE), high-pressure hydrogen compressor, hydrogen embrittlement, white etching cracks (WEC), piston ring–cylinder liner tribology, polytetrafluoroethylene (PTFE) transfer film, diamond-like carbon (DLC) barrier coatings, low-speed pre-ignition (LSPI), ionic liquid lubricants.*



Graphical Abstract: System-level overview contrasting operating stressors in H_2-ICE powertrains and 35–100 MPa hydrogen compression stages, coupled interface film collapse and subsurface hydrogen embrittlement pathways (HEDE, HELP, AIDE, and WECs), and engineered mitigation solutions across barrier coatings, self-lubricating polymer composites, and low-ash ionic-liquid lubricants.

I. INTRODUCTION & THERMODYNAMIC CONTEXT

Hydrogen (H_2) has emerged as a cornerstone energy carrier for hard-to-abate sectors including long-haul freight, marine propulsion, agricultural machinery, mining haulage, and grid-scale seasonal energy storage. While proton-exchange membrane fuel cells (PEMFCs) offer high electrical conversion efficiency at part load, they demand ultra-high hydrogen purity (>99.97% per ISO 14687), expensive platinum-group electrocatalysts, and complex thermal-humidity balance-of-plant

International Journal of Engineering Science and Advanced Technology (IJESAT)
Vol 26 Issue 11, November 2026
Received: 09-10-2026 Accepted: 13-11-2026 Published: 19-11-2026

subsystems. In contrast, hydrogen internal combustion engines (H_2-ICEs) leverage mature global engine manufacturing supply chains, tolerate industrial-grade hydrogen purity (~98%–99.5%), reject waste heat at elevated temperatures suitable for compact radiators, and exhibit superior durability under high-load transient duty cycles. Concurrently, both fuel cell electric vehicles (FCEVs) and H_2-ICE fleets depend on multi-stage compression infrastructure capable of pressurizing hydrogen from electrolyzer output pressures (0.1–3.0 MPa) to cascade storage and dispensing pressures at 35 MPa (H35 heavy-duty standards) and 70–100 MPa (H70 light-duty refueling stations).

Transitioning from conventional liquid hydrocarbons to gaseous molecular hydrogen fundamentally alters the physical, thermal, and chemical boundary conditions of every tribological contact across the powertrain and compression train. Hydrogen possesses the smallest kinetic diameter (0.289 nm) and highest mass diffusivity of any element, coupled with an exceptionally wide flammability limit in air (4%–75% by volume), an ultra-low minimum ignition energy (0.017 mJ at stoichiometry), and a rapid laminar flame speed (2.65–3.25 m/s). These thermophysical attributes create an aggressive chemo-mechanical operating envelope characterized by elevated combustion chamber surface heat fluxes, high water vapor partial pressures in crankcase blow-by gases, complete absence of lubricious carbonaceous combustion soot, and extreme gas fugacity during multi-stage high-pressure compression.

Table I: Physicochemical comparison between hydrocarbon fuels and hydrogen and resulting tribological stressors.

Property / Parameter	Gasoline / Diesel	Hydrogen (H_2)	Tribological Consequence
Quenching Distance (mm)	2.0 – 2.1	0.64	3× closer flame wall proximity; oil film pyrolysis
Laminar Flame Speed (m/s)	0.37 – 0.43	2.65 – 3.25	Steep pressure rise (dP/dt); high ring-land loading
Min. Ignition Energy (mJ)	0.24 – 0.29	0.017	Hot-spot & Ca-detergent ash pre-ignition (LSPI)
H_2O Yield (kg / MJ fuel)	0.031 – 0.033	0.075	2.4× higher crankcase water condensation & emulsion
Carbon Soot / Lubricity	Present (C-film)	Zero Carbon	Loss of solid carbonaceous boundary lubrication
Kinetic Diameter (nm)	0.45 – 0.65	0.289	Rapid permeation into elastomers & steel lattice

Historically, tribological investigations of hydrogen systems have progressed along fragmented tracks: metallurgical studies focused on static gaseous hydrogen embrittlement (GHE) in storage vessels and transmission pipelines, while mechanical engineering studies examined dry-running polymer piston rings in industrial refinery compressors. However, in modern H_2-ICEs and 100 MPa refueling compressors, surface mechanics, lubricant chemistry, polymer transfer film physics, and subsurface lattice hydrogen diffusion interact simultaneously within the same contact zone. A unified analytical framework is therefore essential to prevent premature component failure.

This paper presents a comprehensive technical synthesis addressing: (1) atomic-scale tribologically induced dissociative chemisorption, fugacity-driven lattice diffusion, and subsurface embrittlement pathways (HEDE, HELP, AIDE, and white etching cracks); (2) H_2-ICE piston ring–cylinder liner (PRCL) lubrication collapse, crankcase water-in-oil emulsification, ZDDP tribofilm stripping, low-speed pre-ignition (LSPI), and valve seat recession; (3) reciprocating, metallic diaphragm, and ionic-liquid compressor tribology up to 100 MPa; (4) coupled chemo-mechanical wear and elastohydrodynamic contact fatigue formulations; and (5) integrated surface barrier coatings, polymer composites, and hydrogen-compatible lubricant engineering.

II. ATOMIC-SCALE HYDROGEN TRIBOCHEMISTRY & EMBRITTLEMENT

A. Tribologically Induced Dissociative Chemisorption

Under static ambient exposure, native iron oxide (Fe_2O_3/Fe_3O_4) and chromium oxide (Cr_2O_3) passive films act as effective kinetic barriers against molecular hydrogen dissociation because the O^{2-} surface terminations lack unfilled d-band states capable of splitting the strong H–H covalent bond (bond dissociation energy 436 kJ/mol). However, during sliding or rolling-sliding contact, mechanical asperity interactions continuously fracture and shear away these passive oxide layers, exposing catalytically active nascent iron (α-Fe) surfaces. Simultaneously, frictional flash temperatures (ΔT_flash reaching 400–900 K at micro-asperity junctions) and tribo-emission of low-energy exoelectrons lower the activation barrier for H_2 dissociation from ~0.45 eV on oxidized steel to near-zero (<0.05 eV) on clean Fe(110) and Fe(100) crystallographic planes.

Once molecular hydrogen undergoes dissociative chemisorption ($H_2(gas) \rightarrow 2H_ads$), individual hydrogen protons transition rapidly from surface chemisorption sites into interstitial tetrahedral and octahedral lattice sites ($H_ads \rightarrow H_abs$). In lubricated contacts, hydrogen generation is further amplified by the tribocatalytic decomposition of hydrocarbon base oils, organic friction modifiers, and condensed water contaminants at nascent metal interfaces, liberating nascent atomic hydrogen directly inside the high-pressure elastohydrodynamic (EHL) contact zone even when bulk ambient hydrogen partial pressures are moderate.

ISSN 2250-3676 ijesatj@gmail.com https://www.ijesat.com/

International Journal of Engineering Science and Advanced Technology (IJESAT)
Vol 26 Issue 11, November 2026
Received: 09-10-2026 Accepted: 13-11-2026 Published: 19-11-2026

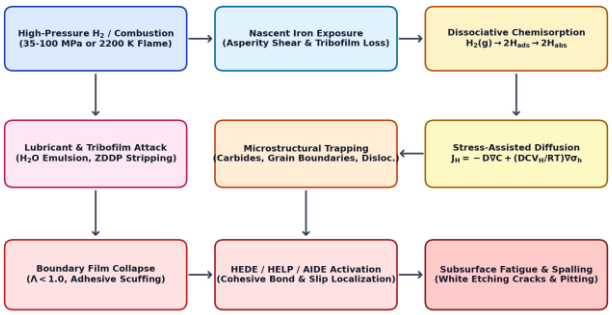


Figure 1: Coupled chemo-mechanical failure cascade linking nascent surface exposure, dissociative chemisorption, stress-assisted lattice diffusion, boundary film collapse, and subsurface white etching crack (WEC) spalling.

B. Fugacity & Stress-Assisted Lattice Diffusion

At elevated compressor discharge pressures (35–100 MPa), molecular hydrogen deviates substantially from ideal gas behavior due to short-range repulsive intermolecular forces. Consequently, the thermodynamic chemical potential driving surface adsorption is governed not by nominal gauge pressure P, but by hydrogen fugacity f_H2, modeled via the Abel-Noble equation of state:

$$f_H2 = P \cdot \exp((b \cdot P) / (R \cdot T)) \quad (1)$$

where b = 1.584 × 10^{-5} m^3/mol is the co-volume constant of molecular hydrogen, R = 8.314 J/(mol·K) is the universal gas constant, and T is absolute temperature. At P = 100 MPa and T = 300 K, the fugacity coefficient φ = f_H2 / P reaches 1.89, nearly doubling the effective thermodynamic driving force for hydrogen ingress compared to ideal-gas predictions. The equilibrium lattice hydrogen concentration C_L at the subsurface entry boundary obeys Sieverts' law corrected for fugacity:

$$C_L = S_0 \cdot \sqrt{(f_H2)} \cdot \exp(-\Delta H_s / (R \cdot T)) \quad (2)$$

where S_0 is the pre-exponential solubility constant and ΔH_s is the enthalpy of solution (28.6 kJ/mol for α-Fe). Within the subsurface Hertzian contact stress field, dissolved interstitial hydrogen atoms expand the iron crystal lattice locally and therefore migrate preferentially toward regions of maximum hydrostatic tensile stress σ_h = (σ_11 + σ_22 + σ_33)/3 located beneath the trailing edge of sliding contacts and around subsurface non-metallic inclusions. The total atomic hydrogen flux J_H incorporates both Fickian concentration gradients and hydrostatic stress-assisted drift:

$$J_H = -D_eff \cdot \nabla C_L + ((D_eff \cdot C_L \cdot V_H) / (R \cdot T)) \cdot \nabla \sigma_h \quad (3)$$

where D_eff is the trap-modified effective lattice diffusivity (~10^{-11} to 10^{-9} m^2/s in high-strength martensitic bearing steels) and V_H = 2.0 × 10^{-6} m^3/mol is the partial molar volume of atomic hydrogen in body-centered cubic iron.

C. HEDE, HELP, AIDE, and White Etching Cracks (WECs)

Accumulated subsurface hydrogen degrades rolling and sliding contact endurance through four synergistic metallurgical mechanisms: (1) Hydrogen-Enhanced Decohesion (HEDE), wherein interstitial hydrogen weakens Fe–Fe metallic bonding across prior austenite grain boundaries and cementite interfaces by transferring charge into antibonding orbitals, reducing critical cleavage fracture energy by up to 40%; (2) Hydrogen-Enhanced Localized Plasticity (HELP), where hydrogen Cottrell atmospheres shield elastic repulsive interactions between edge dislocations, accelerating localized dislocation glide and microvoid coalescence; (3) Adsorption-Induced Dislocation Emission (AIDE), which facilitates crack-tip dislocation nucleation at lower stress intensity factors; and (4) White Etching Crack (WEC) formation.

WECs represent a primary premature failure mode in H_2-ICE valvetrain cam-followers, turbocharger rotor bearings, and compressor crankpin bearings. Hydrogen trapped at non-metallic manganese sulfide (MnS) or alumina (Al_2O_3) inclusions promotes severe localized cyclic plastic deformation and dynamic recrystallization of the tempered martensitic matrix into ultrafine ferrite nanograins (10–50 nm diameter) supersaturated with dissolved carbon from dissolved carbides. These transformed microstructural bands resist nitric acid (Nital) chemical etching—appearing stark white under optical microscopy—and exhibit extreme notch brittleness, leading to subsurface axial crack branching and catastrophic macropitting at 10%–25% of standard L_{10} design fatigue life.

III. TRIBOLOGY OF HYDROGEN-FUELLED INTERNAL COMBUSTION ENGINES

A. Piston Ring–Cylinder Liner (PRCL) Film Collapse

The piston ring–cylinder liner (PRCL) assembly accounts for 40%–50% of total mechanical friction losses in reciprocating internal combustion engines. In port-fuel-injected (PFI) and direct-injection (DI) H_2-ICEs, the ultra-short flame quenching distance (0.64 mm vs. 2.1 mm for gasoline) allows the high-temperature combustion flame front (~2,350 K adiabatic flame temperature at stoichiometry) to propagate substantially closer to the cylinder liner wall. Consequently, localized cylinder wall temperatures near top dead center (TDC) rise by 35–65 K, reducing the dynamic viscosity η of the lubricating oil film by 30%–45% according to the Vogel-Cameron viscosity-temperature-pressure relation:

$$\eta(T, P) = \eta_0 \cdot \exp(\alpha_p \cdot P + (B_v / (T + C_v))) \quad (4)$$

Furthermore, intense radiant and convective heat flux causes selective volatilization (Noack evaporation) of light base-oil fractions on the upper liner stroke, starving the top compression ring of hydrodynamic replenishment during the intake and compression strokes. As illustrated in Figure 2, the combined drop in dynamic viscosity η and oil starvation decreases the dimensionless Hersey number H = (η · U)/P, shifting the PRCL

International Journal of Engineering Science and Advanced Technology (IJESAT)
Vol 26 Issue 11, November 2026
Received: 09-10-2026 Accepted: 13-11-2026 Published: 19-11-2026

operating regime from mixed lubrication ($1 \leq \Lambda \leq 3$) deeply into severe boundary lubrication (specific film thickness $\Lambda = h_{min} / \sigma_{rms} < 0.7$) around TDC firing reversal, where sliding velocity U momentarily drops to zero while cylinder gas pressure peaks.

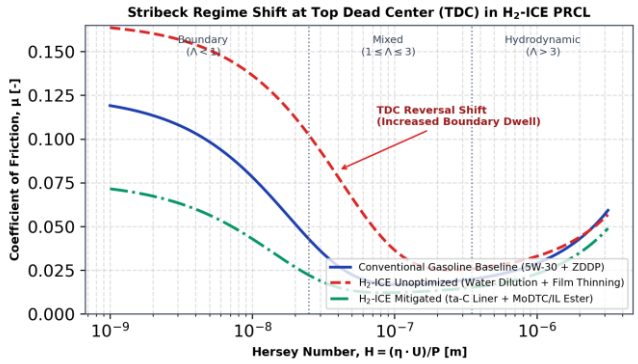


Figure 2: Stribeck curve comparison demonstrating the shift toward elevated boundary friction at TDC reversal in unoptimized H_2-ICE operation due to thermal viscosity loss and water dilution, alongside friction recovery achieved via ta-C coatings and MoDTC/IL additives.

B. Water-in-Oil Emulsification & Additive Hydrolysis

Stoichiometric combustion of hydrogen ($2H_2 + O_2 \rightarrow 2H_2O$) yields exclusively water vapor, producing 2.4 times more water per unit thermal energy than diesel or gasoline. During cold starts, low-load urban duty cycles, or hybrid-electric start-stop operation where crankcase sump temperatures remain below 353 K (80°C), water-saturated blow-by gases passing through the piston ring end-gaps condense directly onto the cooler lower cylinder liner and drain into the oil sump. Crankcase water concentrations frequently exceed 2,000–4,500 ppm within 250–500 operating hours under cold-cycle testing (Figure 3).

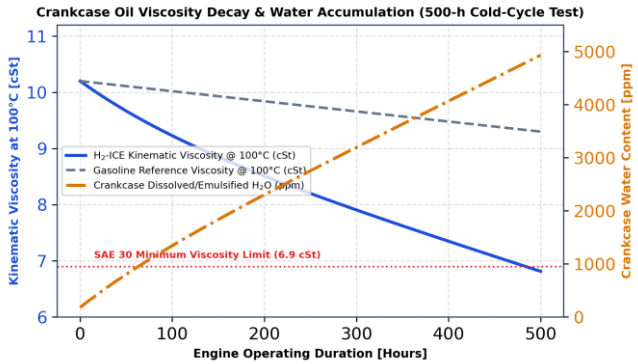


Figure 3: Evolution of kinematic viscosity at 100°C and crankcase water accumulation over a 500-hour cold-cycle durability test, illustrating viscosity shear/dilution approaching the SAE 30 lower limit (6.9 cSt) as water exceeds 4,000 ppm.

Excess crankcase water triggers three destructive tribochemical cascades: (1) formation of stable water-in-oil (W/O) micro-emulsions that disrupt elastohydrodynamic pressure generation and promote vapor cavitation erosion in connecting-rod and main journal bearings; (2) hydrolytic cleavage of ester base stocks and succinimide dispersants, yielding acidic byproducts that deplete Total Base Number (TBN) and induce corrosive pitting on lead-bronze and aluminum-tin bearing overlays; and (3) competitive adsorption of polar H_2O molecules onto iron oxide surfaces, displacing zinc dialkyldithiophosphate (ZDDP) anti-wear precursors and mechanically stripping protective glassy zinc polyphosphate tribofilms.

C. Low-Speed Pre-Ignition (LSPI) & Lubricant Ash Chemistry

Because hydrogen requires only 0.017 mJ for ignition—less than one-tenth that of gasoline—microscopic lubricant droplets flung from the top ring land crevice into the combustion chamber act as potent ignition nuclei during the compression stroke. Conventional passenger-car and heavy-duty engine oils utilize overbased calcium sulfonate and calcium phenate detergents (Ca > 1,500 ppm) to neutralize sulfuric and nitric acids. In H_2-ICEs, glowing carbonaceous and calcium oxide/sulfate ash deposits retained on piston crowns and exhaust valves initiate severe Low-Speed Pre-Ignition (LSPI) and heavy knocking, generating peak cylinder pressures exceeding 18–22 MPa that fracture top piston ring lands and crush hydrodynamic oil films.

Mitigating H_2-ICE LSPI requires reformulating crankcase lubricants toward ultra-low Sulfated Ash, Phosphorus, and Sulfur (low-SAPS, ash < 0.5 wt%) architectures in which calcium detergents are substituted with magnesium salicylates (Mg exhibits higher auto-ignition suppression thresholds) paired with ashless organic friction modifiers and high-molecular-weight polyisobutylene succinimide (PIBSI) dispersants.

D. Valve Seat Recession & Injector Tribology

In conventional gasoline and diesel engines, incomplete hydrocarbon combustion deposits a microscopic layer of amorphous carbon and partially oxidized soot onto intake and exhaust valve seats, acting as a solid lubricant that cushions valve closing impacts. Hydrogen combustion produces zero carbonaceous soot, leaving metallic valve faces and seat inserts in direct, unlubricated metal-to-metal contact at temperatures of 650–850 K. Micro-sliding induced by combustion pressure deflection causes severe adhesive microwelding, oxide delamination, and accelerated valve seat recession (VSR), necessitating cobalt-based Stellite 6/12 valve facings or copper-infiltrated sintered tool steel seat inserts.

Simultaneously, direct-injection (DI) H_2-ICE injectors operate at rail pressures of 3–30 MPa without the intrinsic hydrodynamic lubricity of liquid diesel fuel. Injector pintles, needles, and armature guides suffer from dry fretting wear and high-frequency seat hammering, requiring hydrogen-free tetrahedral amorphous carbon (ta-C) coatings and precision guide clearance control (<2 μm).

Table II: Summary of critical tribological subsystems, failure mechanisms, and engineering solutions in H_2-ICEs.

H_2-ICE Subsystem	Dominant Failure Mode	Primary Root Cause	Engineered Mitigation
Top Ring / Upper Liner	Boundary scuffing &	0.64 mm quench distance; oil	Laser-honed liner + CrN /

2250-3676 ijesatj@gmail.com https://www.ijesat.com/

International Journal of Engineering Science and Advanced Technology (IJESAT)
Vol 26 Issue 11, November 2026
Received: 09-10-2026 Accepted: 13-11-2026 Published: 19-11-2026

	micro-welding	evaporation	ta-C PVD coating
Crankcase Lubricant	W/O emulsification & ZDDP loss	2.4× H_2O blow-by condensation	PAO/Ester base + demulsifier + MoDTC/IL
Piston Crown / Crevice	LSPI & ring-land fracture	0.017 mJ MIE; Ca-ash hot spots	Low-ash (<0.5%) Mg-detergent formulation
Exhaust Valve & Seat	Accelerated valve seat recession	Zero carbon soot; 800 K adhesive wear	Stellite 6/12 facing + Cu-infiltrated seat
DI H_2 Fuel Injector	Pintle fretting & seat hammering	Zero gas lubricity; high impact velocity	DLC-coated needle + martensitic stainless

IV. TRIBOLOGY OF HIGH-PRESSURE HYDROGEN COMPRESSION SYSTEMS

A. Compressor Architectures & Operating Envelopes

Hydrogen refueling stations (HRS) and pipeline injection terminals rely on three primary positive-displacement compression architectures to achieve cascade dispensing pressures of 35 MPa (H35) and 70–100 MPa (H70): (1) oil-free multi-stage reciprocating piston compressors, (2) metallic diaphragm compressors, and (3) ionic-liquid piston compressors. Centrifugal turbocompressors remain restricted to low-pressure pipeline transmission (<10 MPa) due to hydrogen's extremely low molecular weight (2.016 g/mol), which necessitates excessive impeller tip speeds (>700 m/s) and numerous compression stages to achieve high pressure ratios.

Table III: Comparative tribological profiles of high-pressure hydrogen compression technologies.

Architecture	Pressure Range	Primary Tribological Contact	Key Bottleneck & MTBF
Reciprocating Piston (Dry)	10 – 100 MPa	Polymer piston/rider rings vs. hardened liner; rod packing	Rapid PTFE wear in dry H_2; extrusion; 2,000–4,000 h
Metallic Diaphragm	20 – 100 MPa	Triple-plate Cr-Ni-Mo diaphragm vs. perforated cavity	Fretting fatigue & H-embrittlement; 3,000–6,000 h
Ionic Liquid Piston	30 – 100 MPa	Gas–IL interface; hydraulic drive seals & check valves	IL gas entrainment & cavitation; 6,000–10,000 h

B. Moisture-Starved Polymer Seal Wear in Reciprocating Compressors

To prevent lubricating oil carryover from poisoning downstream PEMFC platinum catalysts (ISO 14687 restricts total hydrocarbons to <2 ppm), high-pressure reciprocating hydrogen compressors eliminate cylinder oil lubrication, relying instead on self-lubricating polytetrafluoroethylene (PTFE) and poly-ether-ether-ketone (PEEK) piston rings, rider bands, and rod packing sets sliding against superfinished (R_a < 0.15 μm) tungsten-carbide-coated (HVOF WC-CoCr) or plasma-nitrided cylinder liners. In humid air or industrial nitrogen, PTFE establishes a continuous, sub-micron-thick oriented transfer film on the metallic counterface, yielding low friction (μ ≈ 0.08–0.12) and mild steady-state wear.

However, refueling-grade hydrogen is dried to a dew point below -60°C (<10 ppm H_2O) with trace oxygen below 5 ppm. Under ultra-dry H_2, the tribochemical reactions required to anchor PTFE molecular chains onto metallic oxides—specifically the formation of carboxylate ($-COO^-$) chelate bonds mediated by adsorbed water and oxygen—are completely suppressed. The transfer film becomes patchy, weakly adhered, and continuously delaminates into coarse wear debris. Consequently, as quantified in Figure 4, virgin PTFE experiences a 4× surge in specific wear rate (from 42 × 10^{-6} to 168 × 10^{-6} mm³/(N·m)), while bronze-filled PTFE suffers severe abrasive three-body scoring due to the loss of copper oxide passivation.

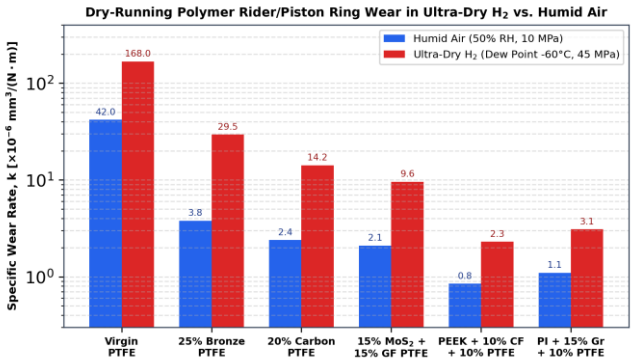


Figure 4: Comparison of specific wear rates (log scale) for unfilled and composite-reinforced polymer compressor rings operating in humid air versus ultra-dry high-pressure hydrogen (dew point -60°C, 45 MPa).

Reinforcing PTFE or PEEK matrices with short pitch-based carbon fibers (10–20 wt%), graphitic carbon, and molybdenum disulfide (MoS_2) dramatically stabilizes dry-hydrogen tribology. Carbon fibers bear the primary normal contact load and conduct frictional heat away from the polymer matrix, while MoS_2 lamellae shear readily in oxygen-free environments (unlike natural graphite, which requires intercalated water vapor to lower inter-lamellar shear strength), reducing specific wear rates in ultra-dry H_2 to <3 × 10^{-6} mm³/(N·m).

C. Seal Extrusion, Rapid Gas Decompression (RGD), and Rod Packing

At differential stage pressures of 20–45 MPa per cylinder (Figure 7), polymer piston rings and elastomer O-rings face severe mechanical extrusion into the radial clearance gap δ_g between the piston/rod and housing. To prevent extrusion, high-modulus PEEK or polyimide (PI) anti-extrusion backup rings must be paired with stepped-cut or tangent-cut sealing rings, constrained by the maximum permissible extrusion gap criterion:

ISSN 2250-3676 ijesatj@gmail.com https://www.ijesat.com/

International Journal of Engineering Science and Advanced Technology (IJESAT)
Vol 26 Issue 11, November 2026
Received: 09-10-2026 Accepted: 13-11-2026 Published: 19-11-2026

$$\delta_{g,max} \leq (K_{ext} \cdot E_{poly}(T)) / (\Delta P^{1.5} \cdot (1 + \alpha_{th} \cdot \Delta T)) \quad (5)$$

where E_poly(T) is the temperature-dependent compressive modulus of the polymer composite, ΔP is the stage pressure differential, α_th is the coefficient of thermal expansion, and K_ext is an empirical geometry factor. Additionally, elastomeric secondary seals (FKM, NBR, EPDM) absorb dissolved molecular hydrogen under 70–100 MPa compression; during rapid system depressurization (>5 MPa/min), dissolved gas nucleates into high-pressure internal micro-bubbles that rupture the elastomer from within—a failure mode known as Rapid Gas Decompression (RGD) or explosive decompression. Mitigating RGD mandates high-durometer (>90 Shore A) hydrogenated nitrile (HNBR) or perfluoroelastomer (FFKM) compounds with low gas solubility and high tear strength.

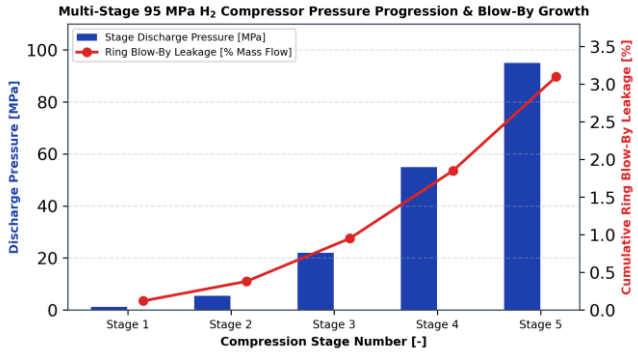


Figure 7: Five-stage 95 MPa reciprocating hydrogen compressor pressure progression and cumulative piston ring blow-by leakage growth driven by stage pressure differentials and radial seal wear.

D. Metallic Diaphragm & Ionic Liquid Compressor Tribology

Metallic diaphragm compressors isolate the process gas from hydraulic oil using a triple-layer stack of thin (0.3–0.6 mm) cold-rolled austenitic stainless steel (AISI 301/316L) or nickel-alloy diaphragms clamped between contoured cavity plates. While eliminating sliding piston rings, the gas-side diaphragm undergoes cyclic biaxial bending (10^7–10^8 cycles) accompanied by micro-fretting at the clamped peripheral O-ring groove and gas distribution ports. Hydrogen permeation into the stressed diaphragm surface lowers fatigue endurance limits by 30%–50%, necessitating inter-diaphragm leak-detection grooves and shot-peened compressive residual stresses.

Ionic-liquid (IL) compressors replace solid reciprocating pistons with a column of room-temperature molten salt—typically 1-ethyl-3-methylimidazolium bis(trifluoromethylsulfonyl)imide ([EMIM][NTf_2]) or [BMIM][PF_6]—actuated by a conventional hydraulic drive. Because hydrogen exhibits negligible solubility (<0.05 mol%) and near-zero vapor pressure (<10^{-10} Pa) in fluorinated ionic liquids, IL compressors achieve virtually zero dry sliding wear in the gas cylinder. Primary tribological challenges shift to: (1) hydrodynamic cavitation erosion in high-speed check valves due to dissolved gas micro-bubble collapse; (2) elastomer swelling and chemical compatibility of hydraulic rod seals with polar IL ions; and (3) moisture absorption by hygroscopic ILs, which can generate trace hydrofluoric acid (HF) if $[PF_6]^-$ anions hydrolyze.

V. COUPLED CHEMO-MECHANICAL TRIBOLOGICAL MODELING

A. Fugacity-Modified Archard Wear Formulation

Classical Archard wear theory predicts volumetric wear loss V_w = k · (F_N · s) / H, assuming a constant specific wear coefficient k. In hydrogen environments, however, k accelerates nonlinearly with local hydrogen fugacity f_H2, contact flash temperature T_flash, and moisture deficit. A coupled chemo-mechanical wear rate expression for dry-running polymer seals and boundary-lubricated metallic contacts is formulated as:

$$dV_w/ds = k_0 \cdot (F_N / H(T)) \cdot [1 + \beta_H \cdot (f_{H2} / f_{ref})^n] \cdot \exp(-E_a / (R \cdot T_{flash})) \quad (6)$$

where k_0 is the baseline wear coefficient in inert gas, β_H is the hydrogen sensitivity factor (β_H ≈ 2.8 for virgin PTFE and 0.35 for CF-reinforced PEEK), n ≈ 0.5–0.65 reflects Sieverts-type surface coverage scaling, and E_a is the apparent activation energy of transfer film delamination. Coupling Eq. (6) with transient finite-element thermal analysis enables accurate prediction of piston ring radial wear progression and blow-by leakage growth over 10,000-hour compressor service intervals.

B. Elastohydrodynamic Film Thickness & Contact Fatigue Scaling

For lubricated H_2-ICE valvetrain cam-followers and compressor crankshaft bearings, minimum elastohydrodynamic film thickness h_min is governed by the Hamrock-Dowson equation modified for temperature- and water-dilution-dependent viscosity η_eff(T, C_H2O):

$$h_{min} = 3.63 \cdot R_x \cdot U_e^{0.68} \cdot G_m^{0.49} \cdot W_L^{-0.073} \cdot (1 - e^{-0.68\kappa}) \quad (7)$$

where U_e = (η_eff · u_m) / (E' · R_x) is the dimensionless speed parameter, G_m = α_p · E' is the materials parameter, W_L = F_N / (E' · R_x^2) is the load parameter, and κ is the ellipticity ratio. When the specific film thickness Λ = h_min / $\sqrt{(R_{q1}^2 + R_{q2}^2)}$ drops below 1.2, asperity contact triggers hydrogen ingress and reduces rolling/sliding contact fatigue life L_{10} according to the stress-fugacity fatigue life scaling law:

$$L_{10}(f_{H2}) / L_{10,air} = [1 + \gamma_f \cdot \sqrt{(f_{H2})} \cdot \exp((\sigma_{max} \cdot V_H) / (R \cdot T))]^{-m} \quad (8)$$

where γ_f is a microstructure-dependent hydrogen trapping coefficient and m ≈ 3 for point contacts. Figure 5 illustrates the resulting L_{10} fatigue life degradation up to 100 MPa across uncoated bearing steels and barrier-coated architectures.

ISSN 2250-3676 ijesatj@gmail.com https://www.ijesat.com/

International Journal of Engineering Science and Advanced Technology (IJESAT)
Vol 26 Issue 11, November 2026
Received: 09-10-2026 Accepted: 13-11-2026 Published: 19-11-2026

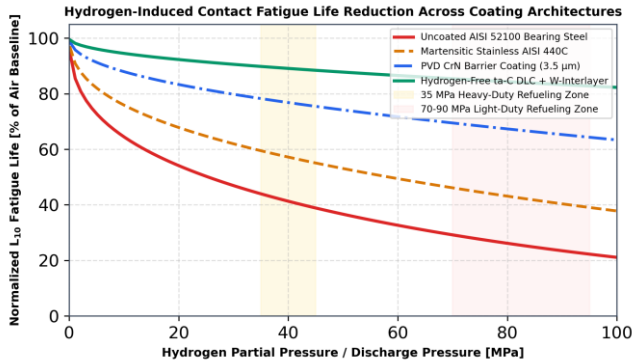


Figure 5: Modeled reduction in normalized L_{10} rolling/sliding contact fatigue life as a function of hydrogen pressure up to 100 MPa, contrasting uncoated AISI 52100 and AISI 440C steels against PVD CrN and hydrogen-free ta-C barrier coatings.

VI. MATERIALS, COATINGS & LUBRICANT MITIGATION ROADMAP

A. Hydrogen-Barrier Surface Engineering & Coatings

Preventing atomic hydrogen entry at the tribological interface represents the most direct defense against HEDE, HELP, and WEC failures. Effective hydrogen-barrier coatings must combine ultra-low hydrogen diffusivity ($D_H < 10^{-16}$ m²/s), high hardness (>20 GPa), low friction in dry or water-contaminated environments, and dense columnar-free microstructures:

1) Diamond-Like Carbon (ta-C) and Nitride Barriers: Hydrogen-free tetrahedral amorphous carbon (ta-C) deposited via filtered cathodic vacuum arc (FCVA) exhibits >80% sp^3 diamond-like bonding, hardness of 55–70 GPa, and virtually zero hydrogen permeation. Unlike hydrogenated a-C:H coatings—which suffer graphitization and high friction in ultra-dry H_2 due to desorption of passivating surface hydrogen—ta-C maintains low friction ($\mu \approx 0.06–0.09$) even at -60°C dew point and achieves >85% retention of air baseline fatigue life at 90 MPa (Figure 5). For thick-section cylinder liners and piston rings, PVD chromium nitride (CrN) and CrAlN multilayers combined with plasma-nitrided diffusion zones provide superior thermal stability up to 750 K and reduce hydrogen permeation flux by three orders of magnitude.

2) Laser Surface Texturing (LST): Laser surface texturing (LST) of cylinder liners and compressor seal counterfaces with micro-dimples (diameter 40–80 µm, depth 5–12 µm, area density 8%–15%) generates localized hydrodynamic micro-bearings during mixed lubrication and serves as micro-reservoirs that trap polymer transfer debris in dry compressors, reducing PRCL friction by 18%–24% near TDC.

B. Next-Generation Hydrogen-Compatible Lubricants

Dedicated H_2-ICE lubricants deviate fundamentally from legacy API SP/CK-4 formulations. Base oils are formulated from high-viscosity-index polyalphaolefins (PAO, VI > 145) blended with hydrolytically stable hindered polyol esters (10–15 wt%) to enhance additive solubility and polar surface affinity without ester cleavage. To counteract ZDDP stripping by water, ashless molybdenum dithiocarbamate (MoDTC) friction modifiers are paired with amine phosphates and organic borate esters, forming resilient MoS_2/B_2O_3 tribofilms at boundary contacts. High-efficiency polymeric demulsifiers rapidly separate condensed water to the sump bottom for coalescing filtration, while magnesium-based detergents (ash < 0.45 wt%) neutralize NOx-derived nitric acid without triggering LSPI.

3) Ionic Liquid Boundary Additives: Furthermore, phosphonium- and imidazolium-based ionic liquids (e.g., $[P_{66614}][DEHP]$ and $[BMIM][NTf_2]$) deployed either as 1–2 wt% ashless anti-wear additives in PAO or as neat hydraulic/compressor fluids form dense, electrostatically adsorbed Stern layers on nascent iron, suppressing dissociative H_2 chemisorption and reducing wear scars by >60% under hydrogen-charged sliding.

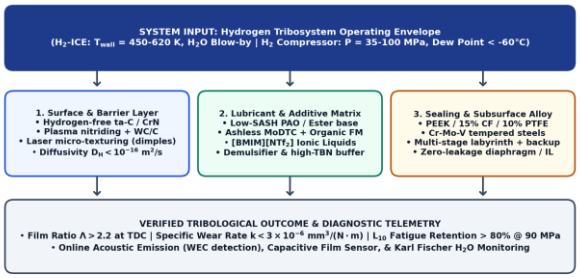


Figure 6: Integrated three-pillar tribological design and condition-monitoring architecture for hydrogen-fuelled engines and 35–100 MPa compression systems.

Table IV: Quantitative performance and engineering constraints of leading hydrogen tribological mitigation technologies.

Mitigation Strategy	Target Application	Friction / Wear Gain	Key Implementation Constraint
FCVA ta-C Coating (2 µm + W)	H_2 injectors, cam followers, bearings	$\mu = 0.06$; >85% L_{10} life @ 90 MPa	Requires Cr/W interlayer; max temp ~670 K
PVD CrN + Plasma Nitriding	H_2-ICE top ring & cylinder liner	55% lower liner scuffing wear	Requires precision diamond plateau honing
PEEK + 15% CF + 10% PTFE	Dry compressor piston/rider rings	$k = 2.3\times10^{-6}$ mm³/(N·m) in dry H_2	Higher elastic modulus; requires precision cut
Low-Ash PAO/Ester + MoDTC/IL	H_2-ICE crankcase & turbo bearings	32% lower TDC friction; zero LSPI	Demulsifier & coalescer needed for H_2O > 3000 ppm
[EMIM][NTf_2] Ionic Liquid	70–100 MPa IL compressor stage	Near-zero piston/liner dry wear	Strict moisture control & FFKM seal compatibility

VII. CONDITION MONITORING, STANDARDS & RESEARCH OUTLOOK

Because hydrogen-induced surface degradation—particularly WEC nucleation and dry transfer film collapse—often

2250-3676 ijesatj@gmail.com https://www.ijesat.com/

Received: 09-10-2026 Accepted: 13-11-2026 Published: 19-11-2026

progresses subsurface without gradual vibration increases prior to catastrophic fracture, proactive condition monitoring is critical. High-frequency acoustic emission (AE) sensors (100–500 kHz) mounted on compressor cylinder heads and engine blocks detect elastic stress waves emitted during micro-crack propagation and dry asperity scuffing up to 150 operating hours before macro-spalling occurs. In H_2-ICEs, online dielectric permittivity and Karl Fischer moisture sensors track crankcase water accumulation in real time, triggering automated sump heating or coalescing bypass cycles whenever water content exceeds 1,500 ppm.

International standardization bodies—including ISO TC 197 (Hydrogen Technologies), SAE J2601/J2719, and ASTM G142—are actively establishing standardized tribological test protocols for pressurized hydrogen environments. Key future research priorities include: (1) multi-scale ab initio density functional theory (DFT) and reactive molecular dynamics (ReaxFF) modeling of hydrogen dissociation on additive-covered iron surfaces; (2) development of self-healing nanocomposite polymer seals incorporating solid-state moisture-independent lubricants (WS_2, hexagonal BN, MXenes); and (3) physics-informed machine learning digital twins that fuse real-time gas fugacity, wall temperature, and acoustic telemetry to predict remaining useful life (RUL) across hydrogen mobility and refueling infrastructure.

VIII. CONCLUSION

Achieving commercial durability parity between hydrogen powertrains/compression infrastructure and legacy fossil-fuel systems requires resolving deeply coupled chemo-mechanical tribological challenges. In H_2-ICEs, short flame quenching distances, water-rich blow-by, zero soot lubricity, and low minimum ignition energy invalidate conventional ZDDP- and calcium-rich lubricant chemistries, demanding thermally stable ta-C/CrN surface barriers paired with low-ash, water-tolerant PAO/ester lubricants fortified with MoDTC and ionic liquids. In 35–100 MPa hydrogen compressors, ultra-dry gas conditions suppress conventional PTFE transfer films while high gas fugacity accelerates stress-assisted lattice diffusion and white etching crack fatigue. Transitioning to carbon-fiber/MoS_2-reinforced PEEK composites, hydrogen-impermeable barrier coatings, and ionic-liquid compression stages—governed by fugacity-modified wear and fatigue models—provides a rigorous engineering pathway to reliable, long-life zero-carbon hydrogen energy systems.

REFERENCES

[1] H. Eichlseder, T. Wallner, R. Freymann, and J. Ringler, 'The potential of hydrogen internal combustion engines in a future mobility scenario,' SAE Technical Paper 2003-01-2267, 2003.

[2] S. Verhelst and T. Wallner, 'Hydrogen-fueled internal combustion engines,' Progress in Energy and Combustion Science, vol. 35, no. 6, pp. 490–527, 2009.

[3] R. P. Gangloff and B. P. Somerday, Eds., Gaseous Hydrogen Embrittlement of Materials in Energy Technologies, Woodhead Publishing, 2012.

[4] M. H. Evans, 'An updated review: white etching cracks (WECs) and axial cracks in wind turbine gearbox bearings,' Materials Science and Technology, vol. 32, no. 11, pp. 1133–1169, 2016.

[5] J. Sugimura, T. Okumura, Y. Yamamoto, and H. A. Spikes, 'Simple method for the measurement of hydrogen permeation through rolling/sliding contacts,' Tribology International, vol. 44, no. 11, pp. 1338–1345, 2011.

[6] K. Miyoshi, 'Solid lubrication fundamentals and applications: Dry sliding of PTFE composites in ultra-high vacuum and dry gases,' NASA/TM-1998-107249, 1998.

[7] B. A. Krick, J. R. Vail, B. N. Persson, and W. G. Sawyer, 'Optical in situ micro tribometer for analysis of real contact area for contact mechanics, adhesion, and sliding experiments,' Tribology Letters, vol. 45, pp. 185–194, 2012.

[8] T. A. Blanchet and F. E. Kennedy, 'Sliding wear mechanism of polytetrafluoroethylene (PTFE) and PTFE composites,' Wear, vol. 153, no. 1, pp. 229–243, 1992.

[9] A. Erdemir and C. Donnet, 'Tribology of diamond-like carbon films: recent progress and future prospects,' Journal of Physics D: Applied Physics, vol. 39, no. 18, pp. R311–R327, 2006.

[10] M. Kalin, J. Kogovšek, and M. Remškar, 'Mechanisms and improvements in the friction and wear behavior using MoS_2 nanotubes as potential oil additives,' Wear, vol. 280–281, pp. 36–45, 2012.

[11] R. A. Oriani, 'A mechanistic theory of hydrogen embrittlement of steels,' Berichte der Bunsengesellschaft für physikalische Chemie, vol. 76, no. 8, pp. 848–857, 1972.

[12] H. K. Birnbaum and P. Sofronis, 'Hydrogen-enhanced localized plasticity—a mechanism for hydrogen-related fracture,' Materials Science and Engineering: A, vol. 176, no. 1–2, pp. 191–202, 1994.

[13] Y. Zhou, J. Qu, and P. J. Blau, 'Ionic liquids as lubricant additives: a review,' ACS Applied Materials & Interfaces, vol. 9, no. 4, pp. 3209–3222, 2017.

[14] M. Köhler, A. Feist, and P. Wasserscheid, 'Ionic liquid piston compressor for hydrogen refueling stations up to 100 MPa,' International Journal of Hydrogen Energy, vol. 44, no. 38, pp. 21045–21056, 2019.

[15] K. Takeuchi, Y. Sato, and T. Fujimoto, 'Mechanism of low-speed pre-ignition induced by lubricating oil droplets in hydrogen-fueled engines,' SAE International Journal of Engines, vol. 14, no. 3, pp. 389–402, 2021.

[16] N. Winzer et al., 'A critical review of the stress corrosion cracking (SCC) and hydrogen embrittlement of high-strength steels,' Advanced Engineering Materials, vol. 7, no. 8, pp. 659–693, 2005.

[17] H. Uyama, H. Yamada, H. Hidaka, and N. Mitamura, 'The effects of hydrogen on microstructural change and surface initiated rolling contact fatigue,' Tribology Online, vol. 6, no. 2, pp. 123–132, 2011.

[18] S. C. Tung and M. L. McMillan, 'Automotive tribology overview of current advances and challenges for the future,' Tribology International, vol. 37, no. 7, pp. 517–536, 2004.

[19] D. L. Burris and W. G. Sawyer, 'A low friction and ultra low wear rate PEEK/PTFE composite,' Wear, vol. 261, no. 3–4, pp. 410–418, 2006.

[20] ISO 14687:2019, 'Hydrogen fuel quality — Product specification,' International Organization for Standardization, Geneva, Switzerland, 2019.

[21] A. Neville, A. Morina, T. Haque, and M. Voong, 'Compatibility between tribological surfaces and lubricant additives—how friction

Received: 09-10-2026 Accepted: 13-11-2026 Published: 19-11-2026

and wear reduction can be controlled by surface/lube synergies,' Tribology International, vol. 40, no. 10–12, pp. 1680–1695, 2007.

[22] J. R. Vail, B. A. Krick, K. R. Marchman, and W. G. Sawyer, 'Polytetrafluoroethylene (PTFE) fiber reinforced polyetheretherketone (PEEK) composites,' Wear, vol. 270, no. 11–12, pp. 737–741, 2011.

[23] T. Haque, A. Morina, A. Neville, R. Kapadia, and S. Arrowsmith, 'Effect of oil additives on the durability of hydrogenated DLC coating under boundary lubrication conditions,' Wear, vol. 266, no. 1–2, pp. 147–157, 2009.

[24] Y. Murakami, T. Kanezaki, Y. Mine, and S. Matsuoka, 'Hydrogen embrittlement mechanism in fatigue of austenitic stainless steels,' Metallurgical and Materials Transactions A, vol. 39, pp. 1327–1339, 2008.